ACS APPLIED MATERIALS & INTERFACES

Research Article

www.acsami.org

Synergistic Effect of Dual Interfacial Modifications with Room-Temperature-Grown Epitaxial ZnO and Adsorbed Indoline Dye for ZnO Nanorod Array/P3HT Hybrid Solar Cell

Dian-Wei Chen, Ting-Chung Wang, Wen-Pin Liao, and Jih-Jen Wu*

Department of Chemical Engineering, National Cheng Kung University, Tainan 701, Taiwan

Supporting Information

ABSTRACT: ZnO nanorod (NR)/poly(3-hexylthiophene) (P3HT) hybrid solar cells with interfacial modifications are investigated in this work. The ZnO NR arrays are modified with room-temperature (RT)-grown epitaxial ZnO shells or/and D149 dye molecules prior to the P3HT infiltration. A synergistic effect of the dual modifications on the efficiency of the ZnO NR/P3HT solar cell is observed. The open-circuit voltage and fill factor are considerable improved through the RT-grown ZnO and D149 modifications in sequence on the ZnO NR array, which brings about a 2-fold enhancement of the efficiency of the ZnO NR/P3HT solar cell. We suggested that the more suitable surface of RT-grown ZnO for D149 adsorption, the chemical compatibility of D149 and P3HT, and the elevated conduction band edge of the RT-grown ZnO/D149-modified ZnO NR array construct the superior interfacial morphology and energetics in the RT-grown ZnO/D149-modified ZnO NR/P3HT hybrid solar cell, resulting in the synergistic effect on the cell efficiency. An efficiency of 1.16% is obtained in the RT-grown ZnO/D149-modified ZnO NR/P3HT solar cell.

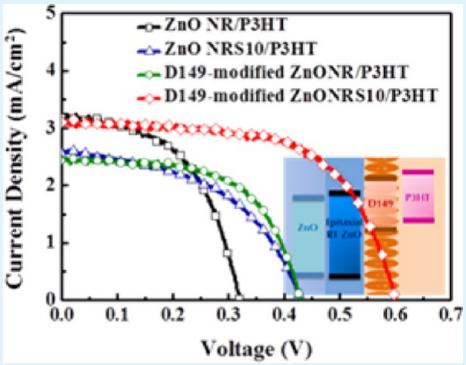

KEYWORDS: *epitaxy, hybrid materials, nanorods, solar cells, zinc oxide*

INTRODUCTION

Bulk heterojunction (BHJ) organic solar cell consists of a randomly distributed electron acceptors in a conjugated polymer matrix.[1] Inorganic nanoparticles (NPs) were the alternatives to fullerene derivatives as electron acceptors for the fabrication of the hybrid polymer−inorganic NP solar cells.[2−7] The active layers of BHJ hybrid solar cells can also be formed by solution processing through mixing NPs with conjugated polymers. Therefore, the BHJ hybrid polymer−inorganic NP solar cells have attracted considerable interest for enhancing the stability of the organic BHJ solar cell.[1] However, similar to the organic BHJ solar cell, the performance of BHJ hybrid cells may be restricted by the poor carrier transport due to deficient connection between the NPs. Thus, a device configuration with ordered and direct path for charge carrier transport to the electrodes is proposed for enhancing the efficiency of the hybrid solar cells.[1]

Because of its anisotropic growth behavior and low crystallization temperature, ZnO nanorod (NR) array deposited on the electrode has been widely used as the ordered electron acceptors/transporter.[8−12] The hybrid active layers were fabricated by infiltrating the conjugated polymers into the interstices of the arrays. However, the highest efficiency of 0.76% is monitored in the hybrid solar cell fabricated using the ZnO NR array and the commonly used conjugated polymer, poly(3-hexylthiophere) (P3HT).[11] Recently, we reported a novel electron acceptor/transporter, i.e., ZnO nanosheet (NS) framework, which is developed from ZnO nanoneedle array on indium tin oxide (ITO) substrate using a room-temperature chemical bath deposition (RTCBD).[13] The ZnO NS framework exhibits an appropriate free space, a faster electron transport rate, and a slightly higher absorption edge in comparison with ZnO NR array. The ZnO NS-P3HT solar cell is therefore demonstrated an efficiency of 0.88%.

In addition to the issue of insufficient interfacial area, the chemical incompatibility between polymer and ZnO NR array, which makes the poor interfacial morphology of the resultant active layer, also restrictions the performances of the ordered heterojunction hybrid solar cell.[7] The device morphology plays a crucial role in the performance of the solar cell because it can significantly influence the charge separation, transport and recombination.[7,14] The performance of the hybrid solar cell has been improved via interfacial modification with dye molecules.[3,15−18] If an applicable interfacial energetics is formed in the dye-modified hybrid solar cell, the dye molecules can contribute to photocurrent other than serving as interfacial modifiers.[15−19] The performances of the ZnO NR/P3HT solar cells have been significantly enhanced by interfacial modifications with indoline dye and squaraine dye individually.[12] The indoline dye possesses dipole moments pointing away from the

Received: April 9, 2013
Accepted: August 12, 2013
Published: August 12, 2013

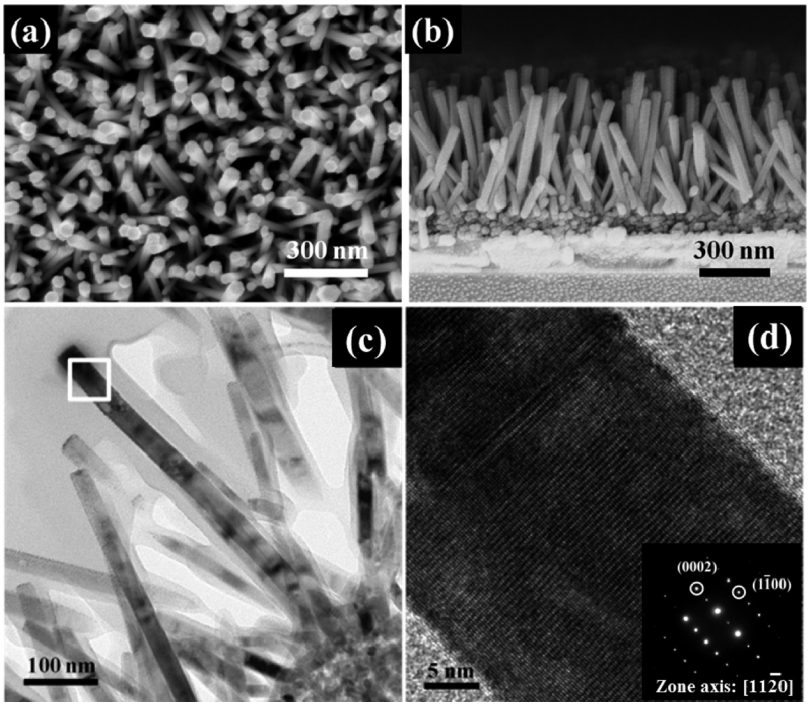

Figure 1. (a) Top-view and (b) cross-sectional-view SEM images of ZnO NR array. (c) Typical TEM image of ZnO NRs. (d) HRTEM image and the corresponding SAED pattern (inset) of an individual ZnO NR.

ZnO surface, resulting in the higher open-circuit voltage (V_{oc}) of the indoline dye-modified ZnO NR/P3HT solar cell. Moreover, the squaraine dye-modified ZnO NR/P3HT solar cell shows improved J_{sc} by extending light harvesting range to near-infrared region. Therefore, the efficiencies of 0.71 and 1.02% were achieved in the indoline dye-modified and squaraine dye-modified ZnO NR/P3HT solar cells, respectively.[12]

We have demonstrated the RT formations of hierarchical nanostructures on ZnO nanowires and nanoneedles to construct ZnO nanocactus array[20,21] and NS framework[13] for use in solar cells. Significant improvements of the photovoltaic performances are achieved by the modifications of the original ZnO nanostructures simply by RT CBD.[22] In the present work, in order to enhance the performance of the ZnO NR/P3HT solar cell, the ZnO NR arrays were modified with RT CBD-grown epitaxial ZnO shells or/and D149 (indoline) dye molecules before the P3HT infiltration. The influences of the modifications on the performances of the hybrid solar cells were investigated. We found a synergistic effect of RT-grown epitaxial ZnO and D149 interfacial modifications on the performance of the ZnO NR/P3HT solar cell. The fill factor (FF) and V_{oc} are considerable improved by the RT-grown ZnO and D149 modifications in sequence, resulting in a 2-fold enrichment of the efficiency of the ZnO NR/P3HT cell. An efficiency of 1.16% is obtained in the RT-grown ZnO/D149-modified ZnO NR/P3HT solar cell. Electrochemical impedance spectroscopy (EIS) was employed to investigate the photocarrier dynamics of the hybrids. The relative conduction band edges (CBEs) of the modified ZnO NR arrays were examined by EIS as well. We suggested that the more fitting surface of RT-grown ZnO for D149 adsorption, the chemical compatibility of D149 and P3HT, and the elevated CBE of the RT-grown ZnO/D149-modified ZnO NR array construct the superior interfacial morphology and energetics in the RT-grown ZnO/D149-modified ZnO NR/P3HT hybrid solar cell, leading to the synergistic effect on the cell efficiency.

EXPERIMENTAL SECTION

A seeded layer for the growth of ZnO NR arrays was first formed on ITO substrate via spin coating.[13,23] The film also performs as the hole blocking layer. The detail for the preparation of the seed layer has been described elsewhere.[13] The ZnO NR arrays were then developed from the seeded layers by a two-batch CBD method using aqueous solution of zinc acetate and hexamethylenetetramine at 95 °C. Brief descriptions of seed layer formation and NR growth are present in Supporting Information. RT CBD of the ZnO epitaxial shells on the ZnO NRs was carried out in an agitated aqueous solution of NaOH and zinc acetate. The solution was prepared using NaOH (5M) and zinc acetate (0.4 M) and consequently diluting by a factor of 10.[13,20,21] The NR arrays modified with D149 molecules were conducted in a 0.5 mM t-butanol/acetonitrile solution of D149 at RT for 1h. Scanning electron microscopy (SEM, JEOL JSM-7000F), transmission electron microscopy (TEM, FEI E.O Tecnai F20 G2MAT S-TWIN), and UV–vis–IR spectrophotometer (JASCO V-670) were employed to respectively examine the morphologies, crystal structures, and optical properties of ZnO NR and modified-ZnO NR arrays.

P3HT infiltration and cell fabrication have been described elsewhere.[13] The details are addressed in the Supporting Information as well. In this work, the exposed areas of all cells with island-type electrodes[24] are 0.03 cm^2. Photovoltaic properties of the solar cells were monitored under AM-1.5 simulated sunlight at 100 mW cm^{-2}.[13] EQE spectra were measured using xenon light source and a monochromator equipped with Si detector.[25] Time-resolved photoluminescence (TRPL) spectroscopy (integrated by Protrustech Corporation Limited) measurements were conducted using a pulse laser (405 nm) with a pulse width of 75 ps for excitation. A time correlated single photon counting (TCSPC) spectrometer was used to record the TRPL decays at 650 nm. The details for EIS measurements are described in the Supporting Information. The chemical capacitances of the ZnO NR arrays,[26] as well as the electron transport and recombination in the hybrid solar cells[27,28] were investigated by fitting the EIS spectra using two-channel transmission line model.

RESULTS AND DISCUSSION

The top-view and cross-sectional-view SEM images of the ZnO NR array grown on ITO substrate are shown in images a and b in Figure 1. The average diameter and length of the NRs are 40 and 500 nm, respectively. The density of the NR array is 1.6×10^{10} cm^{-2}. Figure 1c shows the TEM image of the ZnO NR array on the ITO substrate. The high-resolution (HR) TEM image taken from the denoted region in Figure 1c and the corresponding selected area electron diffraction (SAED) pattern are shown in Figure 1d and its inset, respectively. They reveal that the ZnO NR possesses a single-crystalline structure. Moreover, as displayed in images c and d in Figure 1, the single-crystalline ZnO NR exhibits a smooth surface.

The RT formations of hierarchical nanostructures on the ZnO nanoneedles and nanowires have been demonstrated in our previous works.[13,20,21] Images a and b in Figure 2 show the SEM images of the NR array, which is formed by the modification of the ZnO NR array through a RT CBD for 10 min. The diameter and length of the NR array after the RT CBD for 10 min are increased to 45 and 550 nm, respectively. Typical HRTEM images of an individual ZnO NR after the RT CBD are illustrated in Figure 2c and Figure 2d. They reveal that the original ZnO NR sustains the single-crystalline structure and a thin epitaxial shell is grown on the surface of the original ZnO NR after the RT CBD. For simplicity, the ZnO NR array modified by the RT CBD for 10 min is named as ZnO NRS10 array and the RT-grown epitaxial ZnO shell is named as RT ZnO shell hereafter. The single-crystalline SAED pattern of the ZnO NRS10 shown in Figure 2e confirms the homoepitaxial relationship of ZnO NR and RT ZnO shell. Figure 2f reveals that the thickness of the epitaxial RT ZnO shell formed on the ZnO NR is ~2.5 nm. However, as shown in Figure 2c, d, and f, the epitaxial RT ZnO on the ZnO NR possesses a rough surface, which may be ascribed to the high concentration of NaOH in the RT CBD solution.[20,21]

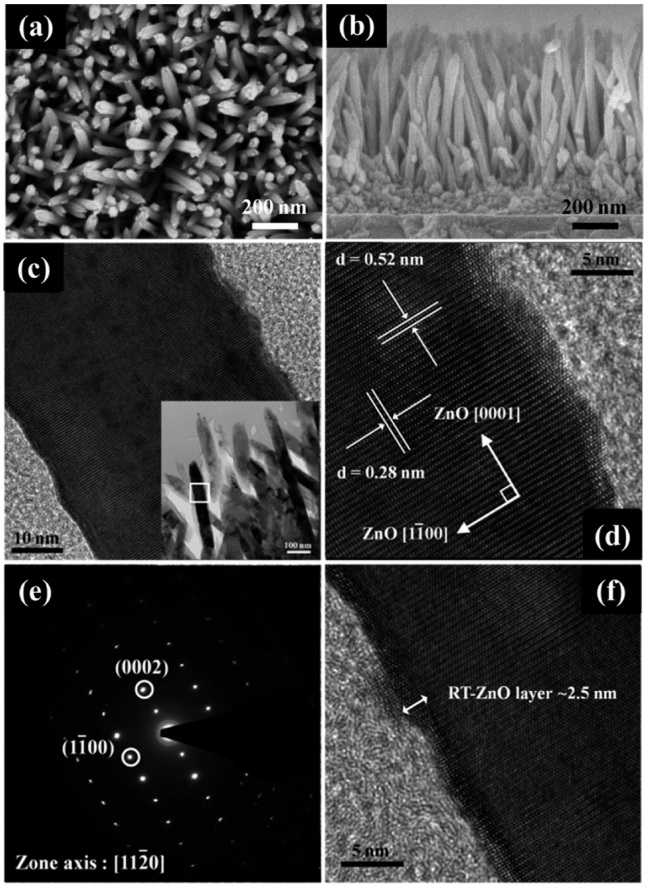

Figure 2. (a) Top-view and (b) cross-sectional-view SEM images of ZnO NRS10 array. (c, d) HRTEM images and (e) the corresponding SAED pattern of ZnO NRS10 of the region denoted in the inset in c. (f) HRTEM image of the ZnO NRS10 revealing epitaxial RT ZnO shell formed on the ZnO NR.

The photocurrent density (J)−voltage (V) curves and photovoltaic properties of the nonmodified ZnO NR/P3HT, D149-modified ZnO NR/P3HT, and ZnO NRS10/P3HT (RT ZnO-modified ZnO NR/P3HT) hybrid solar cells are displayed in Figure 3 and Table 1. They reveal that with interfacial modification using D149 and RT ZnO individually, the open-circuit voltages (V_{oc}) are improved whereas the short-circuit current densities (J_{sc}) are decreased in comparison with those of the nonmodified ZnO NR/P3HT cell. With a slightly decreased fill factor (FF), the efficiency of ZnO NRS10/P3HT cell is comparable to that of nonmodified ZnO NR/P3HT cell. In contrast, the FF is improved in the D149-modified ZnO NR/P3HT cell. A slightly enhanced efficiency is therefore obtained in the D149-modified ZnO NR/P3HT cell.

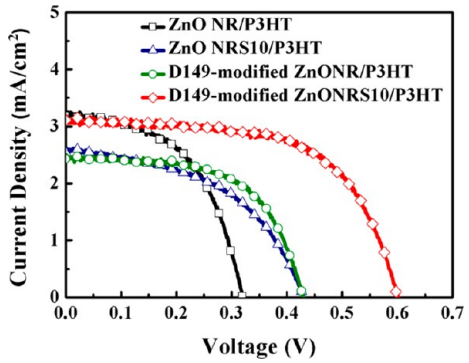

Figure 3. J−V curves of ZnO NR/P3HT, D149-modified ZnO NR/P3HT, ZnO NRS10/P3HT, and D149-modified ZnO NRS10/P3HT hybrid solar cells.

Table 1. Photovoltaic Properties of ZnO NR/P3HT, D149-Modified ZnO NR/P3HT, ZnO NRS10/P3HT and D149-Modified ZnO NRS10/P3HT Hybrid Solar Cells

solar cell	V_{oc} (volt)	J_{sc} (mA/cm^2)	FF	η (%)
ZnO NR/P3HT	0.32	3.20	0.53	0.54
ZnO NRS10/P3HT	0.43	2.55	0.50	0.55
ZnO NR/D149/P3HT	0.43	2.45	0.60	0.64
ZnO NRS10/D149/P3HT	0.60	3.11	0.62	1.16

We have reported that the RT ZnO nanostructures provide more fitting surface for D149 adsorption than bare ZnO NWs do.[20] To improve the J_{sc} of the ZnO NR/P3HT solar cell, the ZnO NR array is modified with RT ZnO and D149 in sequence (i.e., ZnO NRS10 array modified with D149) before the P3HT infiltration. The J-V curve of the D149-modified ZnO NRS10/P3HT hybrid solar cell is also shown in Figure 3. The photovoltaic parameters of the cell are listed in Table 1. Compared to the ZnO NR/P3HT cell, the J_{sc} is not enhanced in the D149-modified ZnO NRS10/P3HT cell as anticipated. Surprisingly, however, the V_{oc} and FF are considerable

improved through the interfacial modifications with RT ZnO and D149 in sequence, resulting in a two-fold improvement of the efficiency of the ZnO NR/P3HT solar cell. It shows a synergistic effect of dual interfacial modifications on the efficiency of the ZnO NR/P3HT solar cell. An efficiency of 1.16% is obtained in the RT ZnO/D149-modified ZnO NR/P3HT solar cell.

As revealed in Table 1, the V_{oc} of the interfacial modified ZnO NR/P3HT solar cells are improved compared to that of the nonmodified ZnO NR/P3HT cell. Especially, an 88% increase of the V_{oc} is attained by the interfacial modifications with both RT ZnO and D149. We have demonstrated that the RT-grown ZnO nanostructures have an elevated conduction band edge (CBE) in comparison with the original ZnO NW array.[21] The relative CBEs of the ZnO NR array and the three modified ZnO NR arrays were also inspected by EIS measurements in the present work. At a given applied voltage, the array with lower CBE will possess a higher chemical capacitance which can be extracted from the EIS spectrum obtained in the dark.[26] Figure 4 reveals the chemical

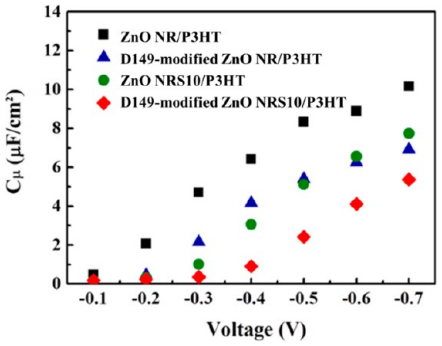

Figure 4. Chemical capacitances of ZnO NR, D149-modified ZnO NR, ZnO NRS10, and D149-modified ZnO NRS10 arrays as a function of applied bias voltage.

capacitances of the four arrays as a function of applied bias voltage. It shows that the positions of the CBEs of the four arrays are in order of D149-modified ZnO NRS10 > ZnO NRS10 ≈ D149-modified ZnO NR > ZnO NR. An upward shift of the CBE in the RT ZnO is also observed in the present work. On the other hand, the D149 molecule adsorbed on the ZnO NR has dipole moment directing away from ZnO surface,[12] which brings about an elevated CBE of the ZnO NR array. The ZnO NRS10 and the D149-modified ZnO NR arrays demonstrate a similar upward shift of the CBE compared to ZnO NR array, which may result in the same increment of the V_{oc} in these two corresponding solar cells as listed in Table 1. However, it should be addressed here that the two interfacial modifications are different in the aspect of physical morphology although their resultant energetics are similar. Unlike the dipole effect on the D149-modified ZnO NR, the ZnO NRS10 is composed of a core−shell structure in which the RT ZnO shell possesses an elevated CBE compared to the ZnO NR core. Moreover, as displayed in Figure S1a (see the Supporting Information), the amount of D149 absorbed on the ZnO NRS10 array is comparable to that on ZnO NR array. Combining the natures of the RT ZnO shell and the adsorbed D149 molecules, as shown in Figure 4, a dramatic reduction of the chemical capacitance is observed in the D149-modified ZnO NRS10 array. It suggests that the CBE of RT ZnO shell is raised further by the D149 modification. The result is consistent with the significant increase of the V_{oc} occurring in the D149-modified ZnO NRS10/P3HT solar cell.

Figure 5 displays the external quantum efficiency (EQE) spectra of the four hybrid solar cells. There are two bands

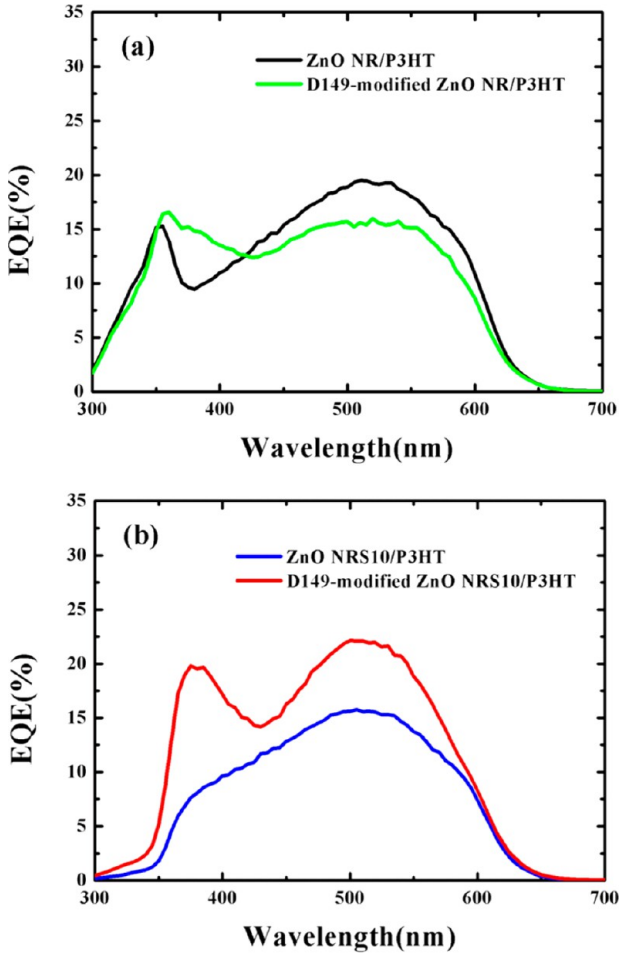

Figure 5. (a) EQE spectra of ZnO NR/P3HT and D149-modified ZnO NR/P3HT hybrid solar cells. (b) EQE spectra of ZnO NRS10/P3HT and D149-modified ZnO NRS10/P3HT hybrid solar cells.

appearing in the EQE spectrum of ZnO NR/P3HT hybrid solar cell, as illustrated in Figure 5a. Compared to the absorption spectra of the ZnO NR array and ZnO NR/P3HT hybrid revealed in Figure S1 (see the Supporting Information), the UV and visible bands in the EQE spectrum of the ZnO NR/P3HT cell are pertaining to the photocurrents from ZnO and P3HT, respectively. As displayed in Figure 5a, the feature of the EQE spectrum of D149-modified ZnO NR/P3HT cell is different from that of the ZnO NR/P3HT cell. In the wavelength range of 360−420 nm, the EQE values are increased in the spectrum of D149-modified ZnO NR/P3HT cell, which is ascribed to the photoelectrons from D149 molecules at the interface as shown in Figure S1 in the Supporting Information. However, the EQE values of the D149-modified ZnO NR/P3HT cell are decreased in the wavelength range of 420−600 nm. It indicates the reduction of photocurrent from P3HT when the interface between ZnO NR and P3HT is modified with D149, resulting in the diminution of the J_{sc} in the D149-modified ZnO NR/P3HT cell, as listed in Table 1.

When the interface between ZnO NR and P3HT is modified with the RT ZnO shell, the UV EQE peak is absent and the

EQE values in the wavelength range of 350−600 nm are decreased as shown in Figure 5b of the EQE spectrum of the ZnO NRS10/P3HT solar cell. Because sunlight distributed in the UV region is only ∼4% of the whole solar spectrum, the reduction of the J_{sc} in the ZnO NRS10/P3HT cell is mainly ascribed to the lower EQE in the wavelength range of 350−600 nm. We also found that the EQE values in the wavelength range of 300−350 nm are dependent on the thickness of the RT ZnO shell as shown in Figure S2 (Supporting Information). The onset wavelength in the UV region is red-shifted when the thickness of RT ZnO shell is increased. The absence of the UV peak in the EQE spectrum of the ZnO NRS10/P3HT solar cell, i.e., the lack of the photocurrent from ZnO NRs, suggests that the valence band edge (VBE) of the RT ZnO shell (with a slightly high band gap) is lower than that of the ZnO NR. Consequently, the transfer pathway for photogenerated holes from the ZnO NR array to P3HT is blocked by the RT ZnO shell at the interface.

When the interface between the ZnO NR and P3HT is modified with RT ZnO and D149 in sequence, the EQE values in the wavelength range of 300−600 nm are higher than those in the ZnO NRS10/P3HT solar cell, as shown in Figure 5b. The onset wavelength in the UV region is slightly blue-shifted in the EQE spectrum of the D149-modified ZnO NRS10/P3HT cell. As illustrated in Figure S3 (see the Supporting Information), the HRTEM images reveal that the RT ZnO shell after dye adsorption is thinner than that of the ZnO NRS10. It is ascribed to the etching of RT ZnO by the acidic dye solution during the D149 adsorption process.[29] Nevertheless, both D149 and P3HT may mainly contribute to the enhanced photocurrents in the wavelength range of 350−600 nm, resulting in the D149-modified ZnO NRS10/P3HT cell possessing a J_{sc} comparable to that of the ZnO NR/P3HT cell.

EIS measurements were performed at V_{oc} under various light intensities to investigate the dynamics of charge recombination at the interface between the ZnO NRs and P3HT in the four hybrid solar cells. The Nyquist plots of the four cells are displayed in Figure S4 (see the Supporting Information). Figure 6 shows the electron lifetimes in the ZnO NR array and ZnO NRS10 array, which are represented as functions of conductivity (σ) in these NR array.[13,25,27] It reveals that the electron lifetimes in the NR arrays of the four solar cells are in order of nonmodified NRS10 > D149-modified NRS10 ≫ D149-modified NR > nonmodified NR, when the conduction bands of the NR arrays possesses the same amount of electrons.

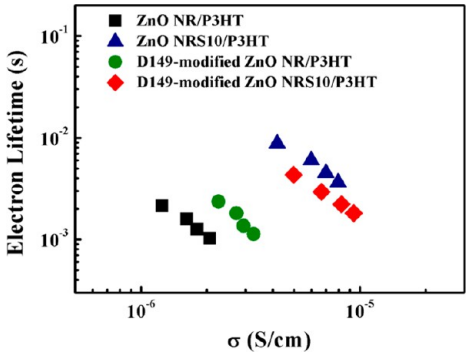

Figure 6. Electron lifetimes as function of conductivity in ZnO NR/P3HT, D149-modified ZnO NR/P3HT, ZnO NRS10/P3HT, and D149-modified ZnO NRS10/P3HT hybrid solar cells.

We have demonstrated that the D149 molecules serve as the recombination barriers at interface between TiO_2 NRs and P3HT to improve the electron lifetime in the TiO_2 NRs.[18,19] In this study, electron lifetimes in the D149-modified ZnO NR/P3HT cell are longer compared to those in the nonmodified ZnO NR/P3HT cell, which also shows the effective recombination barrier of the D149 in the ZnO NR/P3HT cell. As illustrated in Figure 6, the electron lifetimes in the ZnO NRS10/P3HT cell are significantly enhanced in comparison with those in the ZnO NR/P3HT cell, indicating that the thin RT ZnO shell on the ZnO NR functions as a more effective recombination barrier for the ZnO NR/P3HT cell. Moreover, the RT ZnO shell is etched by the acidic dye solution during the D149 adsorption process. A thinner RT ZnO shell therefore exists in the D149-modified ZnO NRS10/P3HT cell, which has been confirmed by the HRTEM images in Figure S3 (see the Supporting Information). Because of the thinner recombination barriers of RT ZnO and D149 in sequence on the ZnO NR surface, the electron lifetimes in the D149-modified ZnO NRS10 cell are slightly shorter than those in the nonmodified ZnO NRS10 hybrid solar cell.

In addition to the change of the interfacial energetics of the ZnO NR/P3HT hybrid, the introduction of the RT ZnO shell into the ZnO NR/P3HT hybrid creates two interfaces to replace the ZnO NR/P3HT one. We suggest that the two interfaces of ZnO NR/RT ZnO and RT ZnO/P3HT possess dramatically different properties (morphologies). Figure S5 (see the Supporting Information) illustrates the TRPL decay curves of the nonmodified ZnO NR/P3HT and the ZnO NRS10/P3HT hybrids as well as the pristine P3HT. The curves are fitted by biexponential decay kinetics.[25] The average PL lifetimes of the pristine P3HT as well as the ZnO NR/P3HT and the ZnO NRS10/P3HT hybrids are 521, 317, and 384 ps, respectively. Compared to the average PL lifetime of 521 ps in the pristine P3HT, the reductions of PL lifetimes in the two hybrids reveals that charge separation is improved once the ZnO NRs exists in the P3HT matrix. The PL lifetime of the ZnO NRS10/P3HT hybrid is longer than that in the ZnO NR/P3HT, showing inferior charge separation efficiency occurred in the ZnO NRS10/P3HT as a result of the RT ZnO interfacial modification. In addition, Figure S6 (see the Supporting Information) shows the cross-sectional SEM images of the ZnO NR/P3HT and ZnO NRS10/P3HT hybrids. For taking the cross-sectional images, the SEM samples were prepared by focused ion beam. The SEM images reveal poor P3HT infiltration in the ZnO NRS10/P3HT hybrid in comparison with that in the ZnO NR/P3HT. It is acribed to the decrease of the free space between the ZnO NRs after the RT ZnO shell deposition. The poor P3HT infiltration and interfacial morphology between P3HT and RT ZnO shell may result in less exciton generation and an inferior charge separation in the ZnO NRS10/P3HT hybrid.

Figure 6 reveals that the ZnO NRS10/P3HT hybrid solar cell exhibits the longest electron lifetime among the four cells. The superior recombination barrier characteristic of the RT ZnO shell is ascribed to both the elevated CBE of the RT ZnO shell and the epitaxial relationship between RT ZnO shell and ZnO NR. There is no grain boundary existing at the interface between the ZnO NR and epitaxially grown RT ZnO shell. With the epitaxial relationship, electron recombination taking place at the interface between the RT ZnO shell and ZnO NR may be negligible. Moreover, the thin RT ZnO layer with an elevated CBE can build an energy barrier to suppress the

electrons in the conduction band of ZnO NR back to recombine with the holes of P3HT. The electron lifetimes in the ZnO NRS10 array are therefore significantly improved. It is concluded that in the ZnO NRS10/P3HT cell, the photocurrent generation at the interface of P3HT and ZnO NR is reduced although the charge recombination is suppressed with the presence of the RT ZnO shell. Combining with the lack of the photocurrent from ZnO NRs due to the lower VBE of the RT ZnO shell, the J_{sc} of the ZnO NRS10/P3HT solar cell is therefore lower than that of ZnO NR/P3HT.

The J_{sc} of the D149-modified ZnO NR/P3HT cell is also lower than that of the ZnO NR/P3HT solar cell, as shown in Table 1. EQE results indicate that the photocurrent originating from P3HT is reduced in the D149-modified ZnO NR/P3HT cell. Because of the incident sunlight from the ITO side of the solar cell as well as the partially overlapping absorption ranges of D149 and P3HT, we suggest that the photons harvested by P3HT are decreased with the presence of D149 at the interface in the D149-modified ZnO NR/P3HT cell. The D149 molecules contribute to the J_{sc}, as shown in the EQE spectrum of the D149-modified ZnO NR/P3HT cell (Figure 5). However, the oxidized D149 molecules may not be regenerated efficiently by P3HT.[30,31] As a hole conductor, P3HT surrounding the oxidized D149 is also oxidized due to its efficient exciton dissociation at the interface. In this aspect, some D149 molecules at the interface of ZnO NR and P3HT may become self-recombination centers. That is, the oxidized D149 is regenerated by the injected electron on conduction band of ZnO NR, resulting in an unsuccessful photon-electron conversion. A smaller J_{sc} is therefore measured in the D149-modified ZnO NR/P3HT cell.

As shown in Table 1, the J_{sc} is improved in the D149-modified ZnO NRS10/P3HT cell compared to those of D149-modified ZnO NR/P3HT and ZnO NRS10/P3HT cells. It should be addressed here that the thickness of the RT ZnO shell is decreased after the D149 adsorption, as confirmed by HRTEM results. It leads to the slight reduction of electron lifetime in the D149-modified ZnO NRS10/P3HT cell in comparison with that of the ZnO NRS10/P3HT cell, as revealed in Figure 6. The proposed energy diagram of the D149-modified ZnO NRS10/P3HT hybrid solar cell is illustrated in Figure 7. The influences of the dual interfacial modifications with RT ZnO and D149 on the interfacial morphology and energetics of ZnO NR/P3HT hybrid are discussed as following by comparing to the modification with RT ZnO and D149 individually. First, the RT ZnO provides more suitable surface for D149 adsorption, which enhances the light harvesting by D149. Therefore, the EQE spectra show that photocurrent from D149 is enhanced in the cell with RT ZnO modification. Moreover, as illustrated in Figure 7, the thin epitaxial RT ZnO layer with an elevated CBE performs as an effective recombination barrier to suppress the injected electrons in the conduction band of ZnO NR back to P3HT. The J_{sc} of the D149-modified ZnO NRS10/P3HT cell is consequently higher than those of the ZnO NRS10/P3HT and D149-modified ZnO NR/P3HT solar cells and is comparable to that of the ZnO NR/P3HT solar cell.

In comparison with the ZnO NR/P3HT solar cell, the V_{oc} and FF are significantly enhanced in the D149-modified ZnO NRS10/P3HT cell. The enhancement of the V_{oc} is ascribed to the elevated CBE of the D149-modified ZnO NRS10 array. The superior FF results from that the epitaxial RT ZnO shell serves as an effective barrier for electron recombination. The

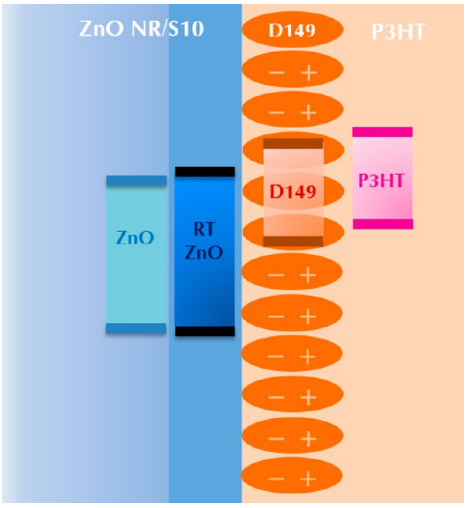

Figure 7. Schematic and energy diagram of D149-modified ZnO NRS10/P3HT hybrid.

synergistic effect of the dye and RT ZnO modifications on the performance of ZnO NR/P3HT cell is thus observed in the present work. The more suitable surface of RT ZnO for D149 adsorption, the chemical compatibility of D149 and P3HT, and the elevated CBE of the D149-modified ZnO NRS10 array construct the superior interfacial morphology and energetics in the D149-modified ZnO NRS10/P3HT cell, bringing about in the 2-fold enhancement of the overall conversion efficiency compared to the ZnO NR/P3HT solar cell.

CONCLUSIONS

The influences of the interfacial modifications on the performances of the ZnO NR/P3HT hybrid solar cells were investigated in this work. The ZnO NR arrays were modified with epitaxial RT ZnO shells or/and D149 dye molecules before the P3HT infiltration. The efficiencies of the hybrid solar cells are not improved due to the decreases of the J_{sc} when the ZnO NR arrays are modified with RT ZnO and D149 individually. A synergistic effect of the RT ZnO and D149 interfacial modifications on the efficiency of the ZnO NR/P3HT solar cell is observed. The J_{sc} of the D149-modified ZnO NRS10/P3HT solar cell is comparable to that of the nonmodified hybrid solar cell. The V_{oc} and FF are considerably improved by the RT-grown ZnO and D149 modifications in sequence, resulting in a 2-fold enrichment of the efficiency of the ZnO NR/P3HT solar cell. The more fitting surface of RT ZnO for D149 adsorption and the chemical compatibility of D149 and P3HT as well as the elevated CBE of the D149-modified ZnO NRS10 array construct the superior interfacial morphology and energetic in the D149-modified ZnO NRS10/P3HT hybrid solar cell. An efficiency of 1.16% is therefore obtained in the D149-modified ZnO NRS10/P3HT solar cell.

ASSOCIATED CONTENT

Supporting Information

Experimental details in seed layer preparation, ZnO NR growth, cell fabrication and EIS measurements, absorption spectra of NR, NRS10, D149, NR/D149, NRS10/D149, NR/P3HT, NR/D149/P3HT, EQE spectra of NR/P3HT, NRS05/P3HT, NRS10/P3HT, HRTEM images of the ZnO NRS10 after dye adsorption, the Nyquist plots of the four hybrid solar cells, the TRPL decay curves of the pristine P3HT as well as the

nonmodified ZnO NR/P3HT and the ZnO NRS10/P3HT hybrids, and cross-sectional SEM images of ZnO NR/P3HT and ZnO NRS10/P3HT hybrids. This material is available free of charge via the Internet at http://pubs.acs.org.

AUTHOR INFORMATION

Corresponding Author

*E-mail: wujj@mail.ncku.edu.tw.

Author Contributions

The manuscript was written through contributions of all authors. All authors have given approval to the final version of the manuscript.

Notes

The authors declare no competing financial interest.

ACKNOWLEDGMENTS

This work was financially supported by the National Science Council, Taiwan under Grant NSC 99-2221-E-006-198-MY3 and NSC 100-2628-E006-032-MY2.

REFERENCES

(1) Mayer, A. C.; Scully, S. R.; Hardin, B. E.; Rowell, M. W.; McGehee, M. D. *Mater. Today* **2007**, *10*, 28−33.

(2) Kwong, C. Y.; Choy, W. C. H.; Djurišić, A. B.; Chui, P. C.; Cheng, K. W.; Chan, W. K. *Nanotechnology* **2004**, *15*, 1156.

(3) Lin, Y. Y.; Chu, T. H.; Li, S. S.; Chuang, C. H.; Chang, C. H.; Su, W. F.; Chang, C. P.; Chu, M. W.; Chen, C. W. *J. Am. Chem. Soc.* **2009**, *131*, 3644−3649.

(4) Li, S. S.; Chang, C. P.; Lin, C. C.; Lin, Y. Y.; Chang, C. H.; Yang, J. R.; Chu, M. W.; Chen, C. W. *J. Am. Chem. Soc.* **2011**, *133*, 11614−11620.

(5) Beek, W. J. E.; Wienk, M. M.; Janssen, R. A. J. *Adv. Mater.* **2004**, *16*, 1009−1013.

(6) Oosterhout, S. D.; Wienk, M. M.; van Bavel, S. S.; Thiedmann, R.; Jan Anton Koster, L.; Gilot, J.; Loos, J.; Schmidt, V.; Janssen, R. A. J. *Nat. Mater.* **2009**, *8*, 818−824.

(7) Weickert, J.; Dunbar, R. B.; Hesse, H. C.; Wiedemann, W.; Schmidt-Mende, L. *Adv. Mater.* **2011**, *23*, 1810−1828.

(8) Olson, D. C.; Piris, J.; Collins, R. T.; Shaheen, S. E.; Ginley, D. S. *Thin Solid Films* **2006**, *496*, 26−29.

(9) Lin, Y. Y.; Chen, C. W.; Chu, T. H.; Su, W. F.; Lin, C. C.; Ku, C. H.; Wu, J. J.; Chen, C. H. *J. Mater. Chem.* **2007**, *17*, 4571−4576.

(10) Lee, Y. J.; Lloyd, M. T.; Olson, D. C.; Grubbs, R. K.; Lu, P.; Davis, R. J.; Voigt, J. A.; Hsu, J. W. P. *J. Phys. Chem. C* **2009**, *113*, 15778−15782.

(11) Baeten, L.; Conings, B.; Boyen, H. G.; D'Haen, J.; Hardy, A.; D'Olieslaeger, M.; Manca, J. V.; Van Bael, M. K. *Adv. Mater.* **2011**, *23*, 2802−2805.

(12) Ruankham, P.; Macaraig, L.; Sagawa, T.; Nakazumi, H.; Yoshikawa, S. *J. Phys. Chem. C* **2011**, *115*, 23809−23816.

(13) Sung, Y.-H.; Liao, W.-P.; Chen, D.-W.; Wu, C.-T.; Chang, G.-J.; Wu, J.-J. *Adv. Funct. Mater.* **2012**, *22*, 3808−3814.

(14) Chen, W.; Nikiforov, M. P.; Darling, S. B. *Energy Environ. Sci.* **2012**, *5*, 8045−8074.

(15) Zhu, R.; Jiang, C. Y.; Liu, B.; Ramakrishna, S. *Adv. Mater.* **2009**, *21*, 994−1000.

(16) Moon, S. J.; Baranoff, E.; Zakeeruddin, S. M.; Yeh, C.-Y.; Diau, E. W.-G.; Gratzel, M.; Sivula, K. *Chem. Commun.* **2011**, *47*, 8244−8246.

(17) Mor, G. K.; Kim, S.; Paulose, M.; Varghese, O. K.; Shankar, K.; Basham, J.; Grimes, C. A. *Nano Lett.* **2009**, *9*, 4250−4257.

(18) Liao, W.-P.; Hsu, S.-C.; Lin, W.-H.; Wu, J.-J. *J. Phys. Chem. C* **2012**, *116*, 15938−15945.

(19) Hsu, S.-C.; Liao, W.-P.; Lin, W.-H.; Wu, J.-J. *J. Phys. Chem. C* **2012**, *116*, 25721−25726.

(20) Wu, C.-T.; Wu, J.-J. *J. Mater. Chem.* **2011**, *21*, 13605−13610.

(21) Jiang, W.-T.; Wu, C.-T.; Sung, Y.-H. *ACS Appl. Mater. Interfaces* **2013**, *5*, 911−917.

(22) Wu, J.-J.; Liao, W.-P.; Yoshimura, M. *Nano Energy* **2013**, http://dx.doi.org/10.1016/j.nanoen.2013.06.018.

(23) Li, C. S.; Li, Y. N.; Wu, Y. L.; Ong, B. S.; Loutfy, R. O. *J. Mater. Chem.* **2009**, *19*, 1626−1634.

(24) Luo, J.; Xiao, L.; Chen, Z.; Gong, Q. *Appl. Phys. Lett.* **2008**, *93*, 133301−3.

(25) Liao, W.-P.; Wu, J.-J. *J. Phys. Chem. Lett.* **2013**, *4*, 1983−1988.

(26) Wang, M.; Grätzel, C.; Moon, S. J.; Humphry-Baker, R.; Rossier-Iten, N.; Zakeeruddin, S. M.; Grätzel, M. *Adv. Funct. Mater.* **2009**, *19*, 2163−2172.

(27) Fabregat-Santiago, F.; Bisquert, J.; Cevey, L.; Chen, P.; Wang, M.; Zakeeruddin, S. M.; Grätzel, M. *J. Am. Chem. Soc.* **2008**, *131*, 558−562.

(28) Garcia-Belmonte, G.; Munar, A.; Barea, E. M.; Bisquert, J.; Ugarte, I.; Pacios, R. *Org. Electron.* **2008**, *9*, 847−851.

(29) Wu, J.-J.; Chen, G.-R.; Yang, H.-H.; Ku, C.-H.; Lai, J.-Y. *Appl. Phys. Lett.* **2007**, *90*, 213109−3.

(30) Yang, L.; Cappel, U. B.; Unger, E. L.; Karlsson, M.; Karlsson, K. M.; Gabrielsson, E.; Sun, L.; Boschloo, G.; Hagfeldt, A.; Johansson, E. M. J. *Phys. Chem. Chem. Phys.* **2012**, *14*, 779−789.

(31) Johansson, E. M. J.; Yang, L.; Gabrielsson, E.; Lohse, P. W.; Boschloo, G.; Sun, L.; Hagfeldt, A. *J. Phys. Chem. C* **2012**, *116*, 18070−18078.